Fluid Dynamics & Materials Processing

Tech Science Press

DOI: 10.32604/fdmp.2022.019772

ARTICLE

Synthesis of a Novel TiO_2@Ag_3PO_4 Core-Shell Structure with Enhanced Photocatalytic Performance

Chao Wei[1,2], Zhongjin Peng[2], Yunfei Chen[3] and Yanhai Cheng[1,*]

[1]School of Mechatronic Engineering, China University of Mining and Technology, Xuzhou, 221116, China

[2]College of Xuhai, China University of Mining and Technology, Xuzhou, 221008, China

[3]Shenyang University of Chemical Technology, Shenyang Economic and Technological Development Zone, Shenyang, 110142, China

[*]Corresponding Author: Yanhai Cheng. Email: weichao@cumt.edu.cn

Received: 14 October 2021 Accepted: 18 December 2021

ABSTRACT

Ag_3PO_4 exhibits a high photocatalytic activity if exposed to visible light, however, it displays bottlenecks such as poor cycle-stability and mediocre ability to degrade methyl orange (MO) because of limited adsorption of MO molecules onto its surface. In this study, nano TiO_2 prepared by a one-step method was combined with Ag_3PO_4 to form a TiO_2@Ag_3PO_4 heterojunction in order to improve this material both in terms of photocatalysis and photostability. After adding a KH-570 silane coupling agent, the photocatalytic performance of TiO_2@Ag_3PO_4 could be improved even further, with the degradation rate of MO maintained at more than 90% after three cycles of visible in light.

KEYWORDS

TiO_2@Ag_3PO_4; heterojunction; photocatalytic performance; methyl orange; silane coupling agent

1 Introduction

The development of material science promotes the progress of human society. With the acceleration of urbanization and industrialization, a series of pollutants (Mercury poisoning [1], Hexavalent chromium [2], Antibiotics [3], etc.) discharged from industrial production, such as waste water, waste gas and waste residue, do far more damage to the environment than the self-purification capacity of the environment, threatening the long-term survival and development of human beings [4,5]. In recent years, photocatalytic materials have become a hot spot in the field of semiconductor research. Semiconductor photocatalytic technology can deal with toxic substances that are difficult to degrade without choice because of its strong oxidation capacity. At the same time, it is environmentally friendly and can use solar energy. Mild reaction conditions, low cost, and no secondary pollution, have broad application prospects. TiO_2 is currently the most widely used photocatalytic material due to its stability, non-toxicity, and low cost. TiO_2 is a wide-bandgap semiconductor. Its band structure is a symmetrical structure along the Brillouin zone. The 3d orbital splits into two sublayers, e_g and t_{2g}, but they are all empty orbitals, and electrons occupy the s and

p energy levels. The meter level is between the s and p bands and the t_{2g} band. The lowest conduction band position is composed of Ti_{3d}, and the highest valence band position is composed of O_{2p} [6,7]. Its forbidden band width is wide, and the absorption of light is mainly concentrated in ultraviolet light, which affects its photocatalytic effect and industrial application [8–11]. Based on this consideration, most researchers combine titanium dioxide with a variety of photocatalytic materials or doped with other ions to modify it. Therefore, new types of photocatalytic materials have become the focus of research in the field of photocatalysis.

In 2010, Yi's research group reported in "Nature Materials" that Ag_3PO_4 has excellent photocatalytic performance. The quantum yield of Ag_3PO_4 under visible light is as high as 90%, and has strong photocatalytic oxidation performance and can decompose pollutants in water. Yi concluded that the indirect band gap of Ag_3PO_4 is 2.36 eV and the direct band gap is 2.43 eV. Under the irradiation of visible light, the rate at which Ag_3PO_4 decomposes water to produce oxygen is much higher than that of $BiVO_4$ and WO_3, and under visible light Ag_3PO_4 also shows strong degradation ability for MB dyes [12]. But because it is slightly soluble in water, Ag_3PO_4 has poor cycle stability and degradation to anionic degradants [13–16].

The silver phosphate surface exhibits a negative surface charge due to the adsorption of OH^- ions [17]. Thus, the cationic dye (RhB or MB) could be easily absorbed onto the catalyst surface by the electrostatic field force, and charge transfer is facilitated. However, for the anionic dye (MO), this effect is not operative as such. Hence, Ag_3PO_4 catalyst is bad at removing the cationic dyes efficiently [9,10,17–22]. In order to improve the photocatalysis and photostability of Ag_3PO_4, nano TiO_2 prepared by one-step method was combined with Ag_3PO_4 to form TiO_2@Ag_3PO_4 heterojunction in this work [23,24].

2 Experiment

2.1 Experiment Reagent

Tetrabutyl titanate ($C_{16}H_{36}O_4Ti$, 99.0%), ethylene glycol ($C_2H_6O_2$, 99%), silver nitrate ($AgNO_3$, ≥99.8%), KH-570 ($C_{10}H_{20}O_5Si$, ≥98.0%), methyl orange ($C_{14}H_{14}N_3NaO_3S$, MO) and diammonium hydrogen phosphate ($(NH_4)_2HPO_4$, ≥99.0%) were purchased from Shanghai Aladdin Biochemical Technology Co., Ltd. (China) Sulfuric acid (H_2SO_4, 95.0%–98.0%), ammonium hydroxide (NH_4OH, 25%–28%), ammonium sulfate [$(NH_4)_2SO_4$, 99.0%], nitric acid (HNO_3, 65.0%–68.0%), ammonium hydroxide (NH_4OH, 25%–28%), edetic acid ($C_{10}H_{16}N_2O_8$, ≥99.5%), isopropanol (C_3H_8O, ≥99.7%), and p-Benzoquinone ($C_6H_4O_2$, ≥98.0%) were from Sinopharm Chemical Reagent Co., Ltd. (Shanghai, China).

2.2 Preparation of Materials

2.2.1 Preparation of TiO_2 Composite

The precursor solution was acquired by adding one milliliter of tetrabutyl titanate to 10 mL of ethylene glycol with 20 min stirring in order to obtain the targeted solution. Then, the targeted mixture was added to the 200 mL of 0.1 mol/L sulfuric acid containing 7 g of ammonium sulfate. The acquisition was immersed in a water bath at 353 K for 1 h. The resulting white pulp was centrifuged, adjusted to neutral with a mixture of ammonium hydroxide and deionized water (volume ratio 1:1). Then, the sample was cleaned with deionized water and vacuum evaporated at 333 K for 2 h.

2.2.2 Preparation of TiO_2@Ag_3PO_4 Composite

Dissolution 0.066 g of $(NH_4)_2HPO_4$ was stirred in 15 ml deionized water for 15 min; a certain amount of titanium dioxide was mixed with the solution of silver nitrate and sonicated for 20 min; 0.255 g of $AgNO_3$ dissolved into 20 ml of deionized water and stirred for 15 min; $(NH_4)_2HPO_4$ solution was slowly added to $AgNO_3$ solution, and the yellow precipitate appeared; a certain amount of dilute nitric acid solution (1:50) was put in the mixed solution, and then the solution was gradually clarified; the clarified solution is placed in

a magnetic stirrer for 15 minutes at a certain temperature, and 1.2 ml of dilute aqueous ammonia (1:10) is slowly added to the solution, kept for half an hour; the yellow sediment was washed away.

The amounts of titanium oxide added herein are 5 mg, 7.5 mg, 10 mg, 15 mg, 20 mg, and 40 mg, respectively.

2.2.3 Modified $TiO_2@Ag_3PO_4$ (M- $TiO_2@Ag_3PO_4$)

120 μl of KH-570 was slowly added dropwise to the above suspension, kept for 30 min, and washed and dried to obtain a modified yellow powder.

2.3 Photocatalytic Activity

45 mg of samples were ultrasonically dispersed in 100 ml of 30 mg/L methyl orange solution for 20 min. The acquisition was stirred for 30 min under the condition of darkness. Photodegradation experiments were performed in an internal photochemical reactor containing 150 W halogen lamp. Under light, 5 ml of solution and catalyst were released every 3 min, and the concentration of residual methyl orange was measured by UV-Vis spectrum.

In the cyclic degradation experiment, 70 mg of Ag_3PO_4 was weighed into 100 ml of 30 mg/L methyl orange, stirred evenly after ultrasonic dispersion, degraded on the self-degradation device. The degraded solution was collected and subjected to a second degradation experiment.

According to the Lambert-Beer law and the variation of the characteristic absorption peak intensity of organic matter, the change of concentration during the degradation process can be calculated quantitatively. Methyl orange has a characteristic absorption peak at 463 nm. The change of absorbance is used to measure the change concentration of methyl orange in degradation solution. C/C_0 (C is the concentration at each reaction time, and C_0 is the initial concentration of methyl orange) was calculated. The degradation curve was plotted with time (t) as abscissa and C/C_0 as ordinate to characterize the degradation rate of photocatalyst.

2.4 Characterization

The X-ray radiation data of XRD and Cu K α 10~80° were collected on the Bruker X-ray diffraction (advance D8), and the scanning speed was 2.4° min^{-1}. The X-ray tube voltage and current were set to 45 kV and 40 mA, respectively. The morphology and chemical composition of the sample were detected by an electron microscope (EOL JEM-100C type from Hitachi, Japan). X-ray photoelectron spectroscopy (XPS) of these materials was recorded in an (Thermo Fisher ESCALAB 250 xi, England) using AlKα radiation (1486.6 eV). Binding energies were calculated with respect to C 1s at 284.8 eV. The measurement accuracy of combined energy is ± 0.05eV. UV−Vis diffuse reflectance spectra were obtained by a JASCO V-570 spectrophotometer equipped with a solid sample holder.

3 Results and Discussion

3.1 XRD of $TiO_2@Ag_3PO_4$

In order to enhance photocatalytic performance of pure Ag_3PO_4, nano TiO_2 particles were directly introduced in the synthesis process of Ag_3PO_4, and $TiO_2@Ag_3PO_4$ composite was further modified by KH-570 silane coupling agent as well. The XRD patterns of Ag_3PO_4, $TiO_2@Ag_3PO_4$, M-$TiO_2@Ag_3PO_4$ were shown in Fig. 1. All samples have similar XRD patterns with respect to silver phosphate (JCPDSno.06-0505); no other obvious phases can be found for $TiO_2@Ag_3PO_4$ and M-$TiO_2@Ag_3PO_4$, which can be attributed to the small amount of added TiO_2 and the formation of core-shell structure on the surface of TiO_2 coated with Ag_3PO_4.

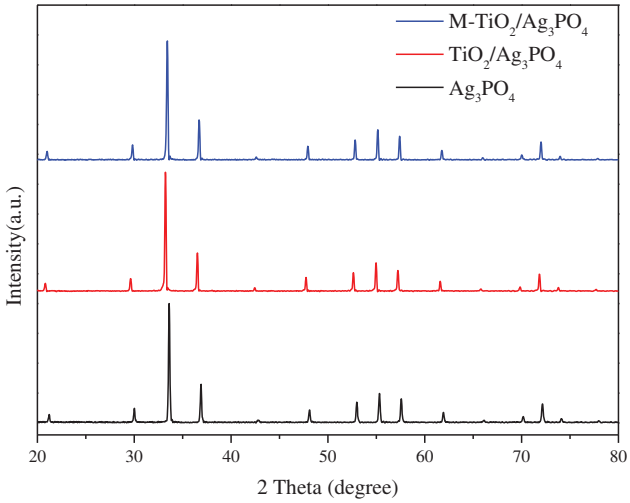

Figure 1: XRD pattern of Ag_3PO_4, TiO_2(7.5 mg)@Ag_3PO_4, M-TiO_2(7.5 mg)@Ag_3PO_4

The intensity of (110) and (200) crystal planes of M-TiO_2@Ag_3PO_4 improves weekly, indicating that the (110) and (200) crystal plane growth was promoted after modification by KH-570.

3.2 Microstructure of TiO_2@Ag_3PO_4

SEM photographs of Ag_3PO_4, TiO_2@Ag_3PO_4, M-TiO_2@Ag_3PO_4 are shown in Fig. 2. The TiO_2 used in this work presents the irregular nano-particle shape with the size range from about 300 nm to 800 nm. After adding TiO_2 in the synthesis of Ag_3PO_4, the morphology of silver phosphate changed to tetrahedron, compared with the polyhedron morphology of pure Ag_3PO_4, which indicates the newly added TiO_2 may act as the nucleation sites of Ag_3PO_4 resulting in the new shape of Ag_3PO_4. M-TiO_2@Ag_3PO_4 shows almost the same morphology as TiO_2@Ag_3PO_4, suggesting KH-570 modification did not destroy the morphology of TiO_2@Ag_3PO_4. The TEM photographs of Ag_3PO_4 and TiO_2@Ag_3PO_4 are shown in Fig. 3. Interestingly, it is found that each particle has a uniform TEM background for the pure Ag_3PO_4 sample, but for TiO_2@Ag_3PO_4 composite, the deeper background can be obviously seen in the center of particles, suggesting the formation of core-shell structure for TiO_2@Ag_3PO_4 composite.

Silver phosphate nucleates and grows with titanium dioxide particles as the nucleation core, and then coats with titanium dioxide particles. Titanium dioxide, which is not the nucleation core of silver phosphate, is adsorbed on the surface of silver phosphate. This structure is a typical core-shell structure.

3.3 XPS

Fig. 4 is the XPS spectrum of TiO_2@Ag_3PO_4. The prepared silver phosphate has Ag, O, P, C elements; the C element is the carbon residue in the XPS instrument; the atomic ratio of Ag:P:O is 33.34:15.82:50.84, close to the stoichiometric ratio of Ag_3PO_4.

The photoelectron binding energies of Ag 3d5/2 and Ag 3d3/2 of Ag_3PO_4 are observed to be 368.08 and 374.08 eV, respectively. The difference between the two peaks is 6 eV, indicating that Ag exists in the form of Ag+.

The O 1s peak of silver phosphate contains an O^{2-} peak of 530.30 eV and a shoulder on the higher binding energy side; the second peak is located at 532.53 eV, caused by chemisorbed oxygen. The lower and higher binding energy peaks have FWHM of 1.31 and 2.19 eV, respectively, and the difference between chemisorbed oxygen and oxygen ion (O^{2-}) binding energy is 1.77 eV. The presence of chemisorbed oxygen can significantly improve the degradation of organic matter in water.

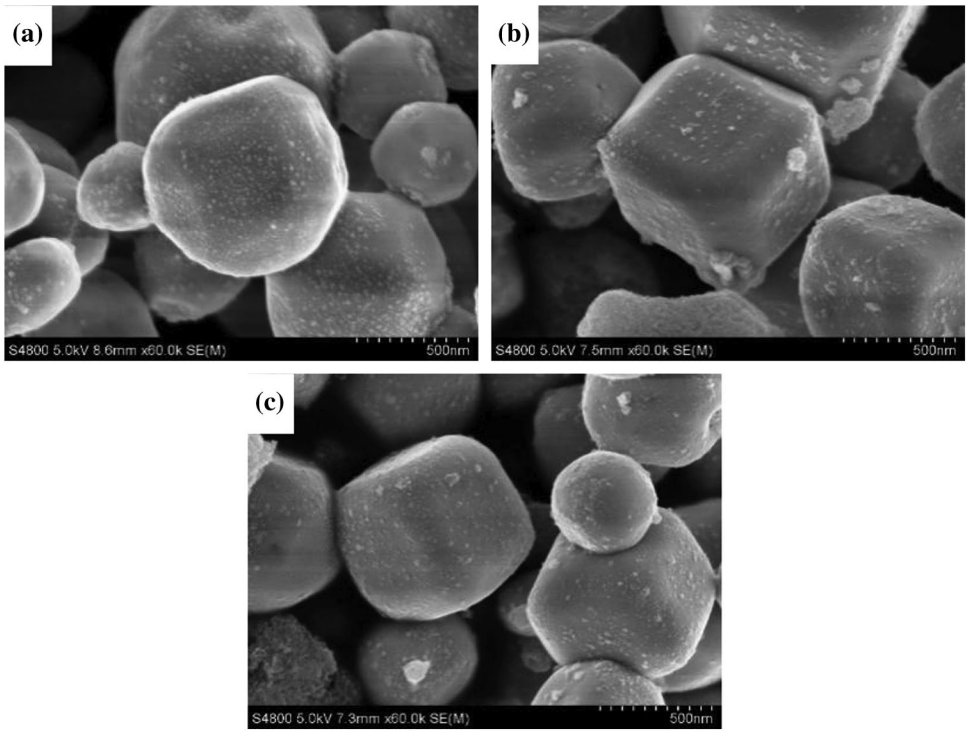

Figure 2: The SEM images of Ag_3PO_4 (a), TiO_2(7.5 mg)@Ag_3PO_4 (b), M-TiO_2(7.5 mg)@Ag_3PO_4 (c)

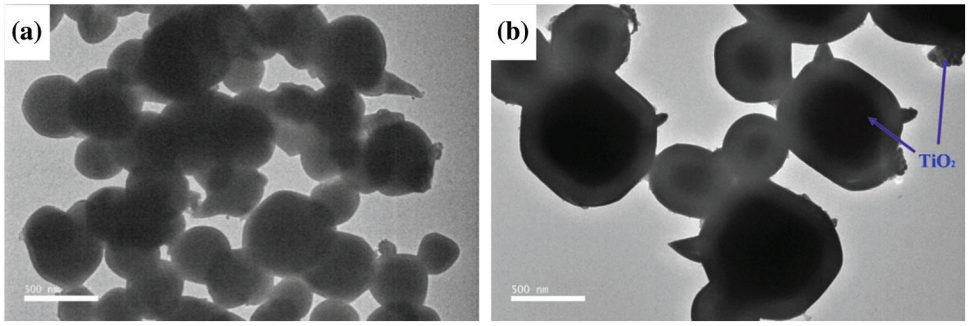

Figure 3: The TEM images of Ag_3PO_4 (a) and M-TiO_2(7.5 mg)@Ag_3PO_4 (b)

The photoelectron binding energies of P 2p3/2 and P 2p3/2 of silver phosphate are 132.91 and 133.81 eV, respectively, and the difference between the two peaks is 0.9 eV, which indicates that P exists in the form of P^{5+}.

3.4 Photocatalytic Performance

Fig. 5 plots the methyl orange degradation curves of Ag_3PO_4, TiO_2@Ag_3PO_4 and M-TiO_2@Ag_3PO_4 under the circumstance of visible light irradiation. The curves reveal that with the increase of titanium dioxide content, the methyl orange degradation of TiO_2@Ag_3PO_4 under visible light is gradually improved, indicating that the addition of titanium dioxide can form a heterojunction with silver phosphate and improve the photocatalytic performance of TiO_2@Ag_3PO_4; when the amount of titanium dioxide added reaches 7.5 mg, the methyl orange degradation of TiO_2@Ag_3PO_4 is optimal, and the degradation rate of methyl orange in 18 min is over 90%; M-TiO_2@Ag_3PO_4 has the obviously enhanced

photocatalytic performance after modification with KH-570, the degradation rate of methyl orange in 15 min can reach 92%, compared to 82% in 15 min for TiO_2@Ag_3PO_4. The reason can be that: (1) the KH-570 surfactant molecules grafted on catalysts can facilitate the absorption of MO molecules and thus promote the improvement of photocatalytic efficiency of TiO_2@Ag_3PO_4 composites; (2) the active facets with high energy increased after adding TiO_2 in the growth of Ag_3PO_4; (3) in order to avoid the accumulation of photogenerated holes in the cores of TiO_2@Ag_3PO_4 particles, some TiO_2 nano particles were loaded on the surface Ag_3PO_4.

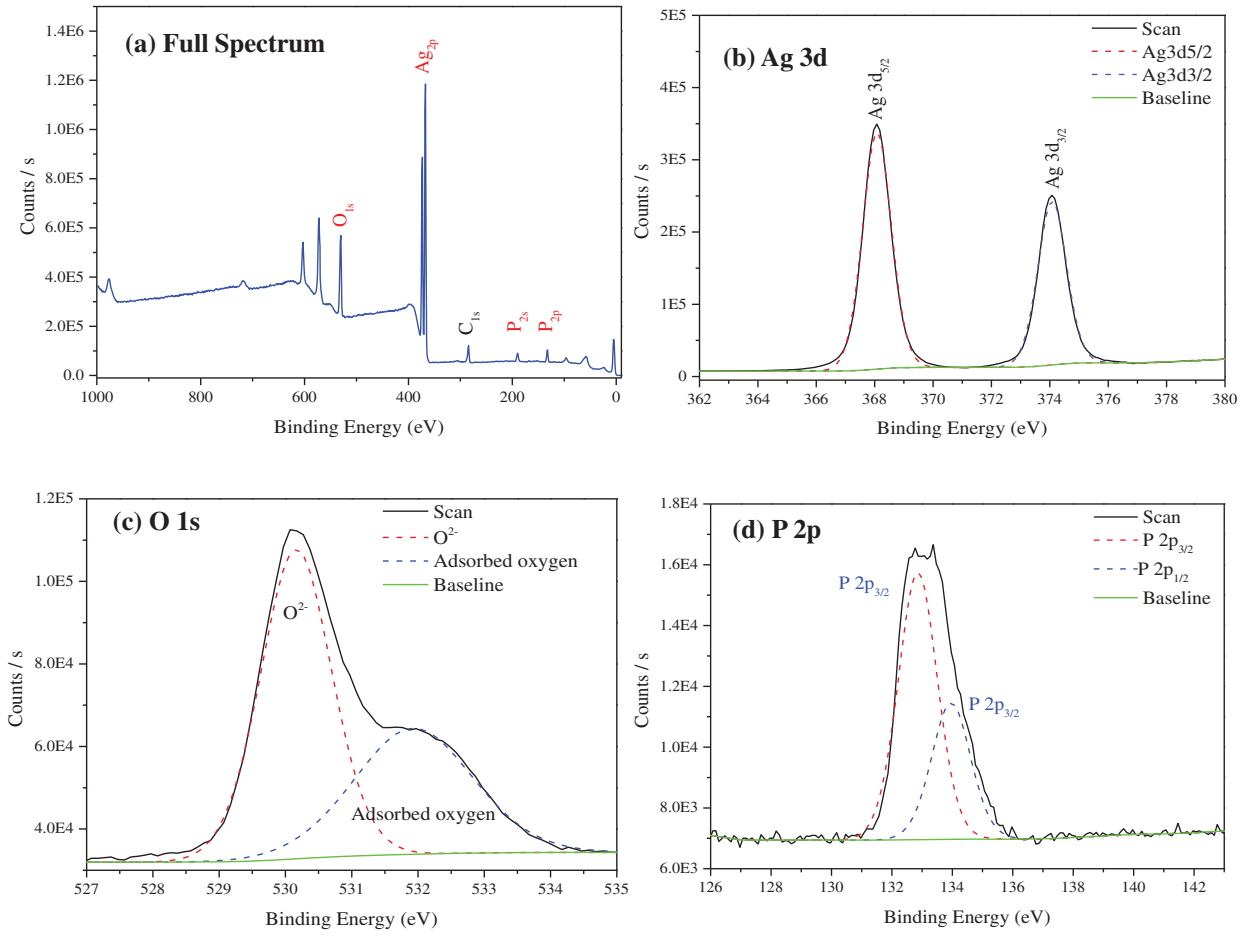

Figure 4: XPS survey AlKα photoelectron spectra of TiO_2(7.5 mg)@Ag_3PO_4

Fig. 6 is the photodegradation kinetic curve. With the increase of the amount of titanium dioxide added, the kinetic k value first increases and then decreases; the kinetic constants (k) are 0.123 min^{-1}, 0.093 min^{-1}, 0.134 min^{-1}, 0.109 min^{-1}, 0.073 min^{-1}, 0.047 min^{-1}. M-TiO_2@Ag_3PO_4 has the highest K value, which is 0.149 min^{-1}.

3.5 Fluorescent Spectrometry

Fig. 7 shows the fluorescence spectra of Ag_3PO_4 and TiO_2@Ag_3PO_4.

As can be seen from the figure, silver phosphate has two emission peaks: 488 nm and 542 nm. According to the intrinsic absorption wavelength of the semiconductor, the band gap widths corresponds to the two emission peaks, 2.55 eV and 2.29 eV, respectively.

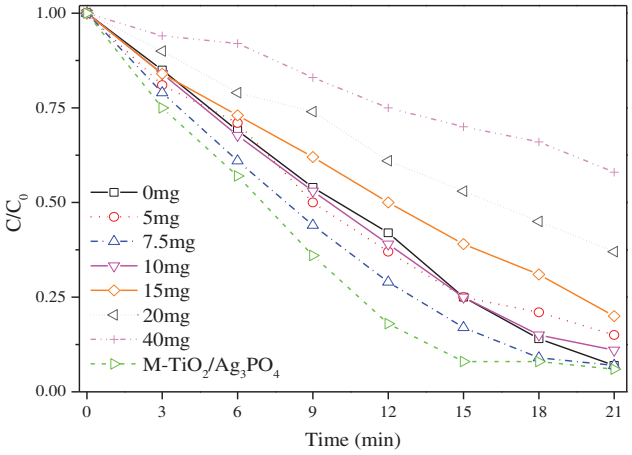

Figure 5: Degradation of methyl orange in different ratios of TiO_2@Ag_3PO_4 under visible light

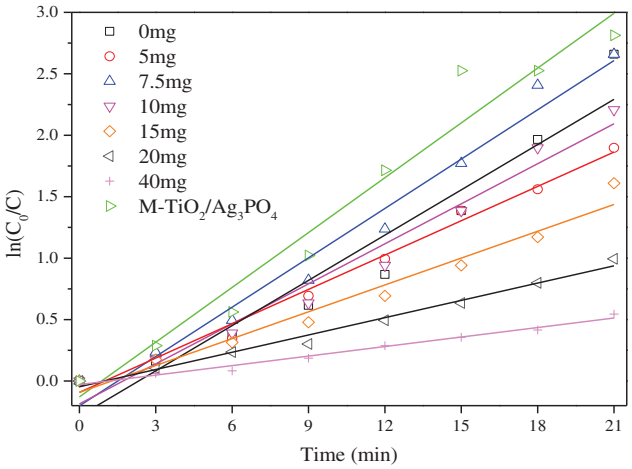

Figure 6: Curve of kinetic constant k of methyl orange in different ratios of TiO_2@Ag_3PO_4 under visible light

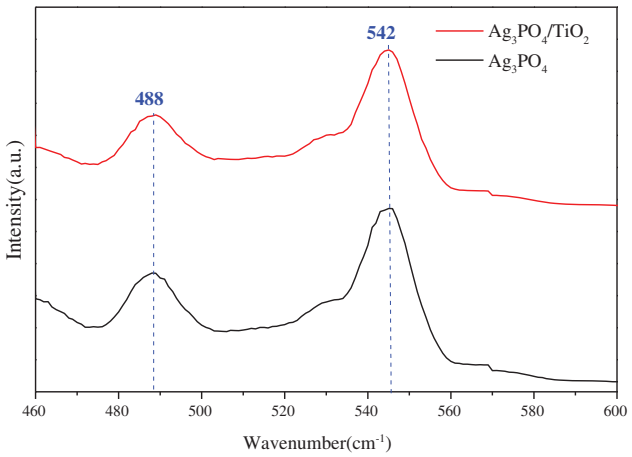

Figure 7: Fluorescence spectra of Ag_3PO_4 and TiO_2(7.5 mg)@Ag_3PO_4

It can be seen that the emission peak at 542 nm is consistent with the gap width of silver phosphate. The emission peak at 488 may be caused by the transition of free carrier band or surface chemisorption oxygen, which is beneficial to the oxidation reaction and the degradation of organic matter.

The emission peak of the composite silver phosphate did not move, because the silver phosphate completely covered the titanium dioxide particles. The emission intensity of TiO_2@Ag_3PO_4 is lower than that of pure Ag_3PO_4 to a certain extent, indicating that the electron-hole recombination probability of TiO_2@Ag_3PO_4 is reduced and its photocatalytic performance is improved.

3.6 DRS and Photocatalytic Mechanism

The absorption intensity and range of Ag_3PO_4 samples can be analyzed by UV-Vis diffuse reflectance spectroscopy. UV spectrophotometry-the comparison of visible light reflection spectra in TiO_2@Ag_3PO_4, M-TiO_2@Ag_3PO_4 and Ag_3PO_4 is shown in Fig. 8a. When Ag_3PO_4 was combined with TiO_2 and TiO_2@Ag_3PO_4 was modified by KH-570, the visible light absorption in TiO_2@Ag_3PO_4 increased significantly (>500 nm).

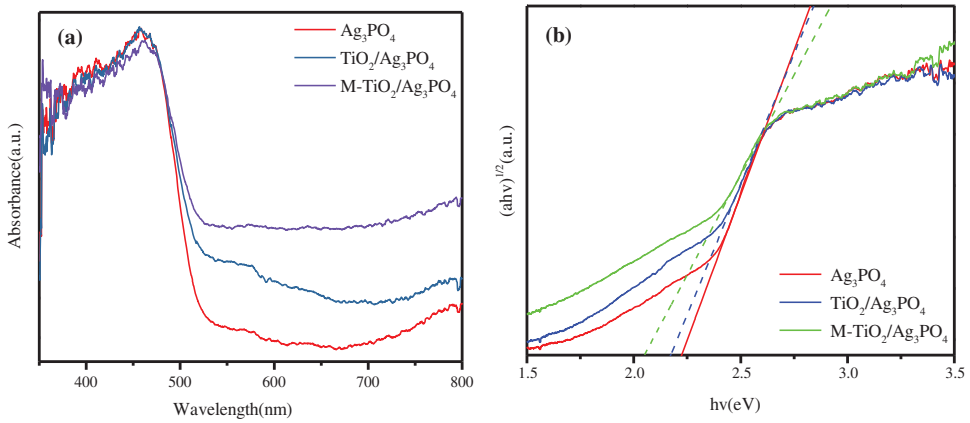

Figure 8: (a) UV−vis diffuse reflectance spectra of TiO_2(7.5 mg)@Ag_3PO_4, modified TiO_2(7.5 mg)@Ag_3PO_4 and Ag_3PO_4. (b) Tauc plot of $(\alpha h\nu)^{1/2}$ *vs.* energy (hν) for TiO_2(7.5 mg)@Ag_3PO_4, modified TiO_2(7.5 mg)@Ag_3PO_4 and Ag_3PO_4

According to formula (1), where a is the absorption coefficient obtained from the test and Eg is the band gap. Using the straight-line extrapolation method, hν is the abscissa, $(ah\nu)^{n/2}$ is the ordinate, and the approximate band gap of the semiconductor is the slope of the fitting line, which is shown in Fig. 8b. The band gaps of the samples are estimated to be 2.23 eV, 2.17 eV and 2.05 eV corresponding to Ag_3PO_4, TiO_2@Ag_3PO_4 and M-TiO_2@Ag_3PO_4. The band gap widths of TiO_2@Ag_3PO_4 and M-TiO_2@Ag_3PO_4 were significantly reduced. The main reason is that the morphology of silver phosphate has changed after compounding and modification [25,26].

$$ah\nu = A\left(h\nu - E_g\right)^{n/2} \tag{1}$$

In order to figure out the photocatalytic process, the band edge position of TiO_2 and Ag_3PO_4 were appraised according to the following empirical formula:

$$E_{VB} = x - E_0 + 0.5E_g \tag{2}$$

$$E_{CB} = E_{VB} - E_g \quad (3)$$

where E_{VB} is the valence band edge potential, E_{CB} is the conduction band edge potential, x is the electronegativity of the corresponding semiconductor, E_0 is the energy of free electrons on the hydrogen scale, and E_g is the band gap energy of the semiconductor. Based upon above equation, titanium dioxide has an E_{CB} of –0.31 eV and an E_{VB} of 2.89 eV; silver phosphate has an E_{CB} of 0.32 eV and an E_{VB} of 2.55 eV. In the case of visible light irradiation, the electrons of TiO_2 and Ag_3PO_4 are excited to the conduction band; the photogenerated electrons and holes are immediately transferred to the conduction band and valence band of Ag_3PO_4; the photogenerated electrons in silver phosphate accumulate at the bottom of the conduction band, and then produce more negative potential electrons, which leads to producing superoxide radical in Fig. 9. Consequently, the photocatalytic performance of TiO_2@Ag_3PO_4 composite is improved. After modification with silane coupling agent, the morphology of silver phosphate was changed and the light absorption capacity was improved [27].

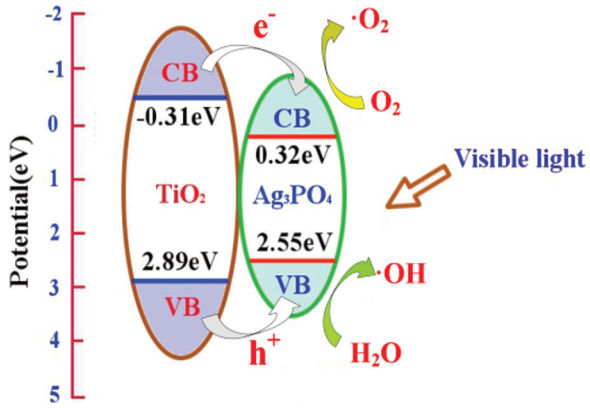

Figure 9: The composite mechanism of TiO_2@Ag_3PO_4

In this paper, ethylenediaminetetraacetic acid (EDTA) was used as the hole trapping agent, isopropanol as the hydroxyl radical trapping agent, and p-benzoquinone as the superoxide radical trapping agent to characterize the active group produced by silver phosphate in the photocatalytic process. The concentration of the trapping agent was 1 mmol/L. Fig. 10 shows the degradation curve of methyl orange of silver phosphate with different trapping agents.

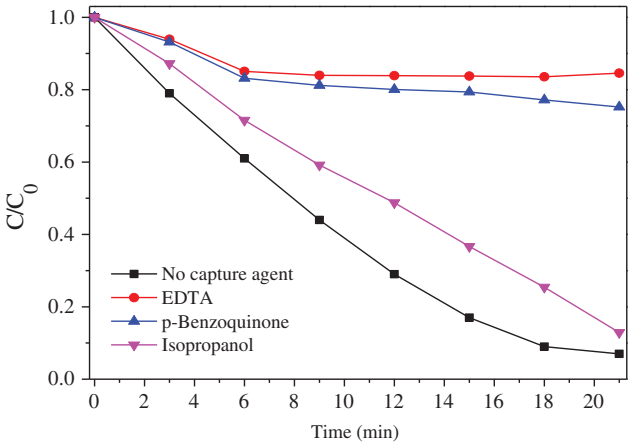

Figure 10: Methyl orange degradation curve of TiO_2(7.5 mg)@Ag_3PO_4 with different capture agents

In order to clarify the main active species in photodegredation of MO, EDTA, isopropanol and p-Benzoquinone were used as hole trapping agents, hydroxyl radical scavenger, and superoxide radical scavenger, respectively. The MO degradation performance of $TiO_2@Ag_3PO_4$ changed little after the addition of isopropanol (Fig. 10). However, the degradation of MO reduced sharply after the addition of EDTA and p-benzoquinone, and just little MO molecules were degraded after 20 min. Clearly, the holes and superoxide radicals are the dominating active groups during the degradation of $TiO_2@Ag_3PO_4$ [28].

3.7 Cycle Stability

Fig. 11 is the cycle degradation curves of methyl orange of modified $TiO_2@Ag_3PO_4$, $TiO_2@Ag_3PO_4$ and Ag_3PO_4. The stability of $TiO_2@Ag_3PO_4$ is improved, and the degradation rate of $TiO_2@Ag_3PO_4$ is maintained at about 70% after three times of degradation, while the degradation rate of Ag_3PO_4 is only 55%. The degradation rate of methyl orange after $TiO_2@Ag_3PO_4$ modified by KH-570 remains above 90%. The silane coupling agent improves the photocatalytic performance and stability of $TiO_2@Ag_3PO_4$. This is because the surface grafted silane coupling agent has a certain hydrophobic function, which prevents the water dissolution and photo-corrosion of silver phosphate.

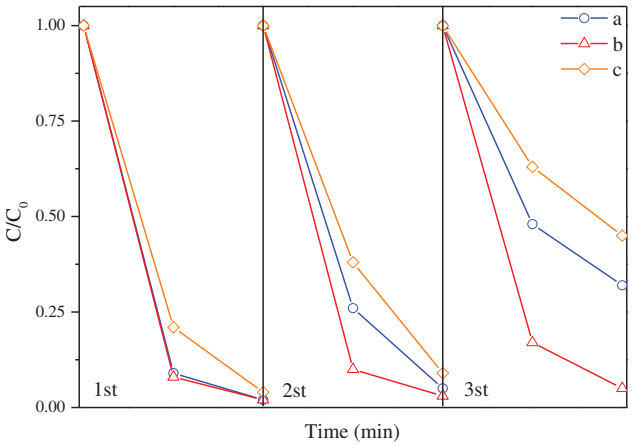

Figure 11: Cyclic degradation curves of $TiO_2@Ag_3PO_4$ (a), modified $TiO_2@Ag_3PO_4$ (b) and Ag_3PO_4 (c) for degradation of methyl orange under visible light

4 Conclusion

On the basis of above mentioned discussion and analysis, a novel $TiO_2@Ag_3PO_4$ composite material have been prepared with success by a simple method. They have been certificated to be highly active photocatalysts and photostability for the degradation of MO under the circumstance of visible light irradiation. Among them, $TiO_2@Ag_3PO_4$ composites added 7.5 mg of TiO_2 forms heterojunction and has the best photocatalytic performance, and its cycle stability is improved; the photocatalytic performance and cycle stability of $TiO_2@Ag_3PO_4$ modified by KH-570 is further improved. After three cycles, the methyl orange degradation rate of $TiO_2@Ag_3PO_4$ modified by KH-570 under visible light remained above 90%. Photogenerated holes and superoxide radical are considered to be the main active species responsible for photocatalytic degradation.

Acknowledgement: We want to acknowledge the advanced analysis $ computation center of China University of Mining and Technology for SEM, XRD and TEM measurements.

Funding Statement: This work was supported by the Natural Science Foundation of the Jiangsu Higher Education Institutions of China (No. 18KJD430009) and the Qing Lan Project of Jiangsu Province.

Conflicts of Interest: The authors declare that they have no conflicts of interest to report regarding the present study.

References

1. Tamiji, T., Nezamzadeh-Ejhieh, A. (2018). A comprehensive study on the kinetic aspects and experimental design for the voltammetric response of a Sn(IV)-clinoptilolite carbon paste electrode towards Hg(II). *Journal of Electroanalytical Chemistry, 829,* 95–105. DOI 10.1016/j.jelechem.2018.10.011.
2. Nosuhi, M., Nezamzadeh-Ejhieh, A. (2017). High catalytic activity of Fe(II)-clinoptilolite nanoparticales for indirect voltammetric determination of dichromate: Experimental design by response surface methodology (RSM). *Electrochimica Acta, 223,* 47–62. DOI 10.1016/j.electacta.2016.12.011.
3. Derikvandia, H., Nezamzadeh-Ejhieh, A. (2017). Increased photocatalytic activity of NiO and ZnO in photodegradation of a model drug aqueous solution: Effect of coupling, supporting, particles size and calcination temperature. *Journal of Hazardous Materials, 321,* 629–638. DOI 10.1016/j.jhazmat.2016.09.056.
4. Du, Q. F., Fang, Z. G. (2021). Analysis of the thermal behavior of a lithium cell undergoing thermal runaway. *Fluid Dynamics & Materials Processing, 17(5),* 887–898. DOI 10.32604/fdmp.2021.016265.
5. Su, K., Deng, S. Q., Li, L. X., Qin, Q. R., Yang, J. Y. et al. (2022). g-C_3N_4 derived materials for photocatalytic hydrogen production: A mini review on design strategies. *Journal of Renewable Materials, 10(3),* 653–663. DOI 10.32604/jrm.2022.018556.
6. Nezamzadeh-Ejhieh, A., Zabihi-Mobarakeh, H. (2014). Heterogeneous photodecolorization of mixture of methylene blue and bromophenol blue using CuO-nano-clinoptilolite. *Journal of Industrial and Engineering Chemistry, 20(4),* 1421–1431. DOI 10.1016/j.jiec.2013.07.027.
7. Ejhieha, A. N., Khorsandi, M. (2010). Photodecolorization of eriochrome black T using NiS-P zeolite as a heterogeneous catalyst. *Journal of Hazardous Materials, 176(1–3),* 629–637. DOI 10.1016/j.jhazmat.2009.11.077.
8. Wei, C., Ying, P., Qiang, Y., Xia, Q., Gu, X. (2019). One-Step synthesis of anatase nanocrystalline TiO_2 at a low temperature for high photocatalytic performance. *International Journal of Electrochemical Science, 14(8),* 7270–7280. DOI 10.20964/2019.08.92.
9. He, H., Jiang, Z., He, Z., Liu, T. (2018). Photocatalytic activity of attapulgite-TiO_2-Ag_3PO_4 ternary nanocomposite for degradation of Rhodamine B under simulated solar irradiation. *Nanoscale Research Letters, 13(1),* 13–28. DOI 10.1186/s11671-018-2443-3.
10. Guo, R., Xia, X., Zhang, X., Li, B., Zhang, H. et al. (2018). Construction of Ag_3PO_4/TiO_2 nano-tube arrays photoelectrode and its enhanced visible light driven photocatalytic decomposition of diclofenac. *Separation and Purification Technology, 200,* 44–50. DOI 10.1016/j.seppur.2018.02.024.
11. Khodami, Z., Nezamzadeh-Ejhieh, A. (2015). Investigation of photocatalytic effect of ZnO-SnO_2/nano clinoptilolite system in the photodegradation of aqueous mixture of 4-methylbenzoic acid/2-chloro-5-nitrobenzoic acid. *Journal of Molecular Catalysis A–Chemical, 409,* 59–68. DOI 10.1080/19443994.2014.922443.
12. Yi, Z., Ye, J., Kikugawa, N., Kako, T., (2010). An orthophosphate semiconductor with photooxidation properties under visible-light irradiation. *Nature Material, 9(7),* 559–564. DOI 10.1038/NMAT2780.
13. Hu, H., Jiao, Z., Yu, H., Lu, G. (2013). Facile synthesis of tetrahedral Ag_3PO_4 submicro-crystals with enhanced photocatalytic properties. *Journal of Materials Chemistry A, 1(7),* 2387–2390. DOI 10.1039/c2ta01151d.
14. Ge, M., Zhu, N., Zhao, Y. P., Li, J., Liu, L. (2012). Sunlight-assisted degradation of dye pollutants in Ag_3PO_4 suspension. *Industrial & Engineering Chemistry Research, 51(14),* 5167–5173. DOI 10.1021/ie202864n.
15. Ma, X. G., Lu, B., Li, D., Shi, R., Pan, C. S. et al. (2011). Origin of photocatalytic activation of silver orthophosphate from First-Principles. *Journal of Physical Chemistry C, 115(11),* 4680–4687. DOI 10.1021/jp111167u.
16. Bi, Y., Ouyang, S., Umezawa, N., Cao, J., Ye, J. (2011). Facet effect of single-crystalline Ag_3PO_4 sub-microcrystals on photocatalytic properties. *Journal of the American Chemical Society, 133(17),* 6490–6492. DOI 10.1021/ja2002132.

17. Wang, H., Bai, Y., Yang, J., Lang, X. (2012). A facile way to rejuvenate Ag_3PO_4 as a recyclable highly efficient photocatalyst. *Chemistry–A European Journal, 18(18),* 5524–5529. DOI 10.1002/chem.201103189.
18. Zhu, C., Zhang, L., Jiang, B., Zheng, J. (2016). Fabrication of Z-scheme Ag_3PO_4/MoS_2 composites with enhanced photocatalytic activity and stability for organic pollutant degradation. *Applied Surface Science, 377,* 99–108. DOI 10.1016/j.apsusc.2016.03.143.
19. Wu, Q., Diao, P., Sun, J., Xu, D. (2015). Draining the photoinduced electrons away from an anode: The preparation of Ag/Ag_3PO_4 composite nanoplate photoanodes for highly efficient water splitting. *Journal of Materials Chemistry A, 3(37),* 18991–18999. DOI 10.1039/c5ta05155j.
20. Yu, H. J., Yu, Y., Liu, J. H., Ma, P. Y., Wang, Y. C. et al. (2015). Space-confined growth of Ag_3PO_4 nanoparticles within WS_2 sheets: Ag_3PO_4/WS_2 composites as visible-light-driven photocatalysts for decomposing dyes. *Journal of Materials Chemistry A, 3(38),* 19439–19444. DOI 10.1039/c5ta04422g.
21. Yang, X., Cui, H., Li, Y., Qin, J., Zhang, R. et al. (2013). Fabrication of Ag_3PO_4-Graphene composites with highly efficient and stable visible light photocatalytic performance. *ACS Catalysis, 3(3),* 363–369. DOI 10.1021/cs3008126.
22. Hu, P. R., Liu, L., An, W. J., Liang, Y. H., Cui, W. Q. (2017). Use of a core-shell composite Ag_3PO_4@TCNQ to improve photocatalytic activity and stability. *Applied Surface Science, 425,* 329–339. DOI 10.1016/j.apsusc.2017.07.003.
23. Mehrali-Afjani, M., Nezamzadeh-Ejhieh, A., Aghaei, H. (2020). A brief study on the kinetic aspect of the photodegradation and mineralization of BiOI-Ag_3PO_4 towards sodium diclofenac. *Chemical Physics Letters, 759,* 137873–137882. DOI 10.1016/j.cplett.2020.137873.
24. Babaahamdi-Milani, M., Nezamzadeh-Ejhieh, A. (2016). A comprehensive study on photocatalytic activity of supported Ni/Pb sulfide and oxide systems onto natural zeolite nanoparticles. *Journal of Hazardous Materials, 318,* 291–301. DOI 10.1016/j.jhazmat.2016.07.012.
25. Nezamzadeh-Ejhieh, A., Bahrami, M. (2015). Investigation of the photocatalytic activity of supported ZnO-TiO_2 on clinoptilolite nano-particles towards photodegradation of wastewater-contained phenol. *Desalination and Water Treatment, 55(4),* 1096–1104. DOI 10.1080/19443994.2014.922443.
26. Jafari, S., Nezamzadeh-Ejhieh, A. (2017). Supporting of coupled silver halides onto clinoptilolite nanoparticles as simple method for increasing their photocatalytic activity in heterogeneous photodegradation of mixture of 4-methoxy aniline and 4-chloro-3-nitro aniline. *Journal of Colloid and Interface Science, 490(1),* 478–487. DOI 10.1016/j.jcis.2016.11.087.
27. Raeisi-Kheirabadi, N., Nezamzadeh-Ejhieh, A. (2020). A Z-scheme g-C_3N_4/Ag_3PO_4 nanocomposite: Its photocatalytic activity and capability for water splitting. *International Journal of Hydrogen Energy, 45(58),* 33381–33395. DOI 10.1016/j.ijhydene.2020.09.028.
28. Ghattavi, S., Nezamzadeh-Ejhieh, A. (2020). GC-MASS detection of methyl orange degradation intermediates by AgBr/g-C_3N_4: Experimental design, bandgap study, and characterization of the catalyst. *International Journal of Hydrogen Energy, 45(46),* 24636–24656. DOI 10.1016/j.ijhydene.2020.06.207.